



Matoa leaf extract mediated synthesis of Se-doped ZnO nanoparticles and their photocatalytic capability

Ari Sulisty Rini^{1,*}, Medinia Putri Simatupang¹, Yolanda Rati², Rahmi Dewi¹

¹Department of Physics, Faculty of Mathematics and Natural Sciences, University of Riau, 28293, Pekanbaru, Indonesia

²Department of Physics, Faculty of Mathematics and Natural Sciences, Bandung Institute of Technology, 40132, Bandung, Indonesia

Received 8 June 2023; Received in revised form 6 November 2023; Accepted 11 January 2024

Abstract

In this work, ZnO-based powders were synthesized by a simple biosynthesis method using matoa leaf extract and microwave irradiation. The pure ZnO was modified with selenium doping (5, 10 and 15 at.%) to improve the photocatalytic capability in degrading 4-nitrophenol. The synthesized powders had wurtzite structure and XRD analysis demonstrated a change in ZnO lattice parameters with Se doping. Granular surface morphology and decrease in particle size with Se doping were observed by using FESEM. Meanwhile, EDX confirmed the presence of Zn, O and Se elements in the doped samples and BET analysis showed that the specific surface area ranged from 10 to 18 m²/g. The observed strong absorption in UV region decreases with Se doping from 367 to 357 nm and is accompanied by an increase in the bandgap energy from 3.14 to 3.23 eV. Under UV irradiation, the ZnO powder doped with 5 at.% Se revealed the highest degrading reaction rate of -0.0218 min^{-1} and photocatalytic efficiency of 88.4% compared to other samples. Therefore, it was shown that an optimal amount of Se and simple biosynthesis route can enhance the photocatalytic capability of ZnO.

Keywords: Se-doped ZnO, structure, 4-nitrophenol, photocatalytic activity, UV irradiation

I. Introduction

The current increase in water pollution is due to the industrial waste usually containing phenolic compounds such as paint, plastic and paper [1]. Several methods such as biodegradation, adsorption, Fenton degradation and wet air oxidation degradation have been reported to treat water pollution [2–4]. These technologies have many drawbacks due to their lengthy reaction times, high operational costs and poor waste decomposition ability [5]. Simple, effective and environmentally friendly ways can be carried out during the degradation process using semiconductor-based photocatalysts. The photocatalysis method utilizes photons as a trigger energy source to degrade pollutants into simpler substances such as CO₂ and H₂O using a catalyst [6].

ZnO, TiO₂, Fe₂O₃, SnO₂, WO₃, In₂O₃ and ZrO₂ are usually used in the photocatalysis process, but some of these materials have limitations in light absorption and

charge separation [7]. ZnO is the most popular photocatalyst material due to its strong oxidizing ability, broad light absorption, high photosensitivity and photostability [8]. In addition, ZnO has a wide band gap (3.37 eV) and high exciton binding energy (60 meV) [9]. However, the small surface area and low photoluminescence capacity are the drawbacks of this material [10]. Therefore, it takes a lot of effort to improve physical properties of ZnO through doping and obtain new characteristics, such as increased optical absorption and surface area, as well as reduced charge recombination and modified crystal lattice structure.

The types of dopant include elements of group III (B, Al, Ga, In, Ti), IV (C, Si, Ge, Sn, Pb) and VI (S, Se, Te, Po) [11]. However, a metal dopant is less effective because of the high charge carrier recombination and is unresponsive under visible light [12]. On the other hand, a non-metal is superior because it has a broad absorption capacity in visible light so it can reduce the recombination charge of ZnO [13]. It is important to underline that Te and Po are toxic, rare and can cause

*Corresponding author: tel: +62 812 7046 4974
e-mail: ari.sulisty@lecturer.unri.ac.id

damage to the crystal lattice. Doping of ZnO with Se exhibits an increase in the band gap and changes the photoelectric properties [14]. The high reduction potential of Se is considered a favourable condition for extracting photo-excited electrons from the conduction band that can facilitate the formation of reactive oxygen [15]. It was reported [16] that Se-doped ZnO synthesized by the seed-mediated hydrothermal method has improved optical and electrical properties. Se-doped ZnO was also synthesized by the facile green method that increased its biological activity [17].

Recently, researchers have begun using plant extract-based biosynthesis, which is environmentally safe, low-cost, short reaction time and non-toxic [18]. Physical and chemical processes generate toxic waste, expensive operational costs and complicated production [19]. Plant extracts have been utilized for ZnO biosynthesis as well as doping, such as biduri leaves (*Calotropis gigantea*) [20], pineapple fruit (*Ananas comosus*) [21] and dragon fruit skin (*Hylocereus polyrhizus*) [22]. Antioxidant compounds in plant extracts serve as capping and stabilizing agents for nanoparticles [23].

In this study, Se-doped ZnO powders were synthesized using matoa leaf extract as a capping agent and applied in photocatalysis. Matoa leaf (*Pometia pinnata*) was chosen due to its high levels of flavonoids, phenols and saponins [24]. In addition, matoa leaf can be easily found in the ground. Efficiency of Se-doped ZnO was examined by degradation of 4-nitrophenol (4-NP) pollutant under UV irradiation. 4-NP is a toxic and carcinogenic phenolic compound. It can cause damage to the central nervous system and liver, weakening the heart-beat to death [25]. This contaminant must be handled seriously so as not to cause environmental issues. The effect of Se doping on ZnO was studied through changes in the crystal structure, morphology, elemental composition, surface area, absorption spectra, band gap energy and photocatalytic activity. The selected environmentally friendly method is capable of producing Se-doped ZnO particles for water purification applications.

II. Experimental

2.1. Biosynthesis of Se-doped ZnO

Matoa leaves were dried under sunlight, mashed and weighed (4 g). Then, they were dissolved in 200 ml of boiled water for 10 min and filtered using Whatman paper. Furthermore, 0.5 M of $\text{Zn}(\text{NO}_3)_2 \cdot 6\text{H}_2\text{O}$ (HIMEDIA® GRM691-500G) was mixed with 20 ml of matoa leaf extract and corresponding amount of Se-doping solution, previously prepared by reacting selenium powder (Loba Chemie) with 0.472 g of NaBH_4 (97% extra pure). The obtained solution was stirred at 1000 rpm until homogeneous. Then, the solution was irradiated using microwave oven at power of 540 W until the precipitate was obtained. The precipitated particles were centrifuged at 4000 rpm for 10 min, washed three times in water, dried at 110 °C and finally annealed at 400 °C for 2 h. In this work, different Se amounts were

used, including 0, 5, 10 and 15 at.% and corresponding sample names were ZSe-0, ZSe-5, ZSe-10 and ZSe-15, respectively.

2.2. Characterization technique

Optical properties were characterized using an Agilent Cary 60 UV-Vis spectrophotometer in 200–700 nm range. Crystal structure was analysed with a Rigaku Miniflex 60 Benchtop Diffractometer and $\lambda_{\text{CuK}\alpha} = 1.541 \text{ \AA}$. Surface morphology and elemental composition were identified using FESEM - EDX Quanta FEG 650 with 20,000× magnification. Surface area as well as pore volume were measured using BET Quantachrome Novatouch LX-4 with degas temperature of 300 °C. The presence of different functional groups was confirmed with a Shimadzu IR Prestige-21 spectrophotometer in 400–4000 cm^{-1} range.

2.3. Photocatalytic experiments

Efficiency of the prepared Se-doped ZnO powders was examined by degradation of 4-nitrophenol (4-NP) solution under UV irradiation. 10 ppm 4-NP was prepared and 5 M NaOH was dripped until pH = 11. Then, 10 mg of catalyst was dissolved and added together with 2 ml H_2O_2 . The suspension was stirred at 1000 rpm in the dark condition for 60 min to achieve an adsorption-desorption equilibrium between the 4-NP solution and the catalyst surface [28]. Next, it was irradiated under 4 UV-C lamps (Krisbow T5 UVC, 8 Watt) for 120 min. To investigate degradation, 5 ml of solution was regularly sampled and measured by UV-Vis absorbance spectra. An illustration of the photocatalysis test process for 4-NP can be seen in Fig. 1.

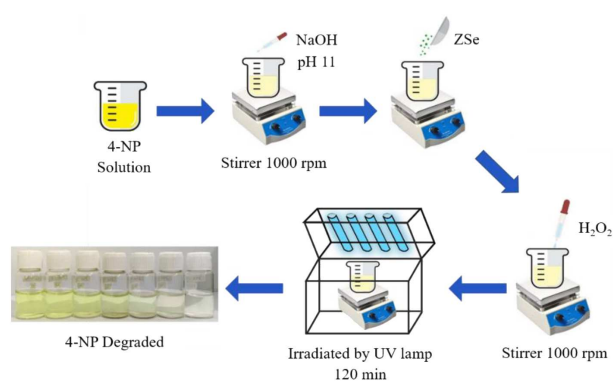


Figure 1. Degradation mechanism of 4-NP by Se-doped ZnO photocatalyst

III. Results and discussion

3.1. Structural analysis

XRD patterns of the ZSe samples are shown in Fig. 2. Diffraction peaks at $2\theta = 32^\circ, 34^\circ, 36^\circ, 47^\circ, 56^\circ, 63^\circ, 66^\circ, 68^\circ$ and 69° corresponded to the planes (100), (002), (101), (012), (110), (013), (200), (112) and (201), respectively. This indicates the presence of hexagonal wurtzite ZnO phase (COD No. 96-210-7060) with space

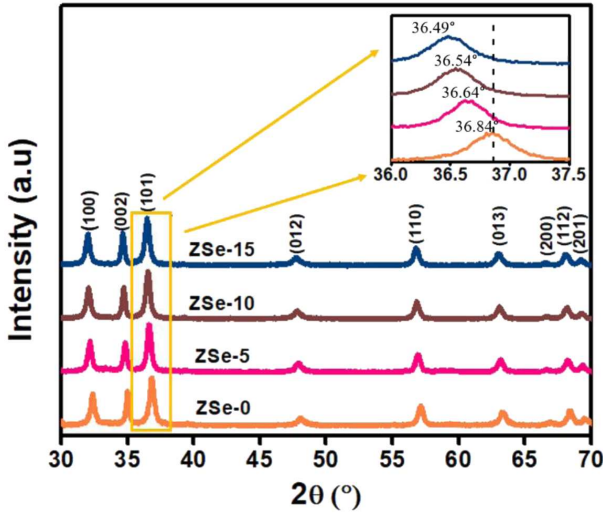


Figure 2. XRD patterns of Se-doped ZnO powders

Table 1. Lattice constants and crystallite sizes of Se-doped ZnO

Sample	2θ [°]	β [°]	Lattice constant		D [nm]
			a [Å]	c [Å]	
ZSe-0	36.84	0.437	3.201	5.123	19.2
ZSe-5	36.64	0.359	3.218	5.150	23.3
ZSe-10	36.54	0.384	3.226	5.165	21.8
ZSe-15	36.49	0.428	3.231	5.173	19.5

group $P6_3mc$ [28]. The absence of other peaks in the XRD spectra suggests that the Se was incorporated in the ZnO structure.

The addition of Se causes the diffraction peak shift towards a smaller 2θ . This occurs due to the larger ionic radius of Se than O so the incorporation of Se into the ZnO lattice causes distortion of crystal structure or lat-

tice stretching [16]. Lattice constants were obtained by Eq. 1 and average crystallite size (D) was calculated from the full width half maximum value (β) using the Debye-Scherrer formula (Eq. 2):

$$\frac{1}{d^2} = \frac{4}{3a^2}(h^2 + k^2 + h \cdot k) + \frac{l^2}{c^2} \quad (1)$$

$$D = \frac{0.9 \cdot \lambda}{\beta_{hkl} \cdot \cos \theta} \quad (2)$$

where d , hkl , a and c , λ , and θ are the distance between the planes, the Miller indices, lattice constants, the X-ray wavelength (1.541 Å) and the diffraction angle, respectively [29].

The calculated values are given in Table 1. It can be seen that the average crystallite size and the lattice constants of the Se-doped ZnO samples increase with Se addition. As it was mentioned, Se doping causes a stretching of ZnO lattice and changes the lattice constants [30]. These changes can affect the band gap energy values and particle sizes of materials [19].

3.2. Surface morphology

FESEM images of the ZSe samples at a magnification of 20,000× are shown in Fig. 3. The surface morphology of all ZSe samples was found to be irregular and varied with doping concentration. With increasing Se content, the ZnO particle size decreases and the distribution becomes more uniform. Coarse grain particles with less homogeneous structure are characteristic of the ZSe-0 sample, whereas the ZSe-5 powder exhibits a granular shape with relatively uniform particle size distribution. The samples with higher Se-content ZSe-10 and ZSe-15 have smaller particle sizes and larger agglomerates. These observations confirm that the percentage of Se doping affected the formation and characteris-

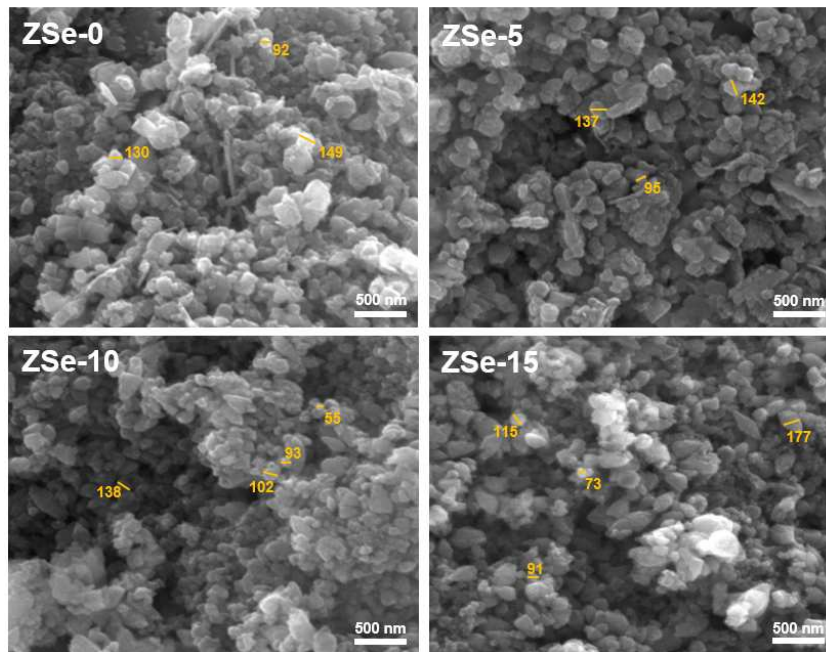


Figure 3. Surface morphology of Se-doped ZnO powders

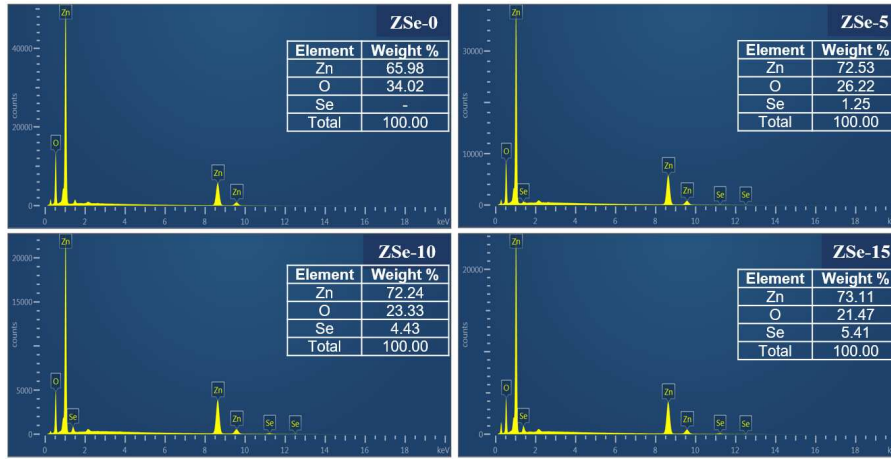


Figure 4. EDX spectra of Se-doped ZnO powders

tics of ZnO nanoparticles [31]. Similar results were also obtained by Song *et al.* [32] who synthesized Se/ZnO based on *Aloe vera* extract.

3.3. Elements composition

The EDX spectra in Fig. 4 confirm the presence of Zn, O and Se elements and provide quantitative information on the composition of the ZSe samples. It proves that the Se-doped ZnO was successfully synthesized. Zn is the most dominant element with the highest peak compared to the other two elements. The ZSe-0 sample does not contain Se and atomic percentage of Se increases with the doping. On the other hand, O element has only one peak whose intensity decreases with doping (i.e. substitution of O with Se).

3.4. Optical analysis

Figure 5a shows the UV-Vis absorbance spectra of the matoa leaf extract and ZSe samples. Matoa leaf extract has an absorption peak at a wavelength of 275 nm. Similar results were also obtained for *Rosmarinus officinalis* extract that indicates absorption of extracts containing antioxidant compounds [18]. The ZSe samples show strong absorption in the UV region (350–370 nm)

that gradually weakens in the visible light region (370–700 nm). This characteristic is in accordance with the optical absorption of ZnO at 370 nm [26]. The absorption peak shifts to the left (blueshift) from 367 nm (for the ZSe-0 sample) to 357 nm (for the ZSe-15 sample) with increasing Se concentration. This indicates that there is a combined reaction between ZnO and Se which causes a quantum confinement effect [17].

The band gap energy in the ZSe sample was determined by the Tauc plot method using the following equation:

$$(\alpha \cdot h \cdot \nu)^2 = A(h \cdot \nu - E_g) \quad (3)$$

where h is the Planck constant, ν is the frequency, α is the absorption coefficient, E_g is the band gap energy and A is the proportionality constant [27]. This method involves extrapolating the curve between $(\alpha \cdot h \cdot \nu)^2$ and photon energy ($h \cdot \nu$) and then identifying the point where it intersects the x -axis at $y = 0$. This intersection point represents the band gap energy of a material.

The band gap energy curves and extrapolated values of E_g for the ZSe samples are shown in Fig. 5b. The Se-doped samples have wider band gap energy than the pure ZnO. This indicates that the addition of Se affects

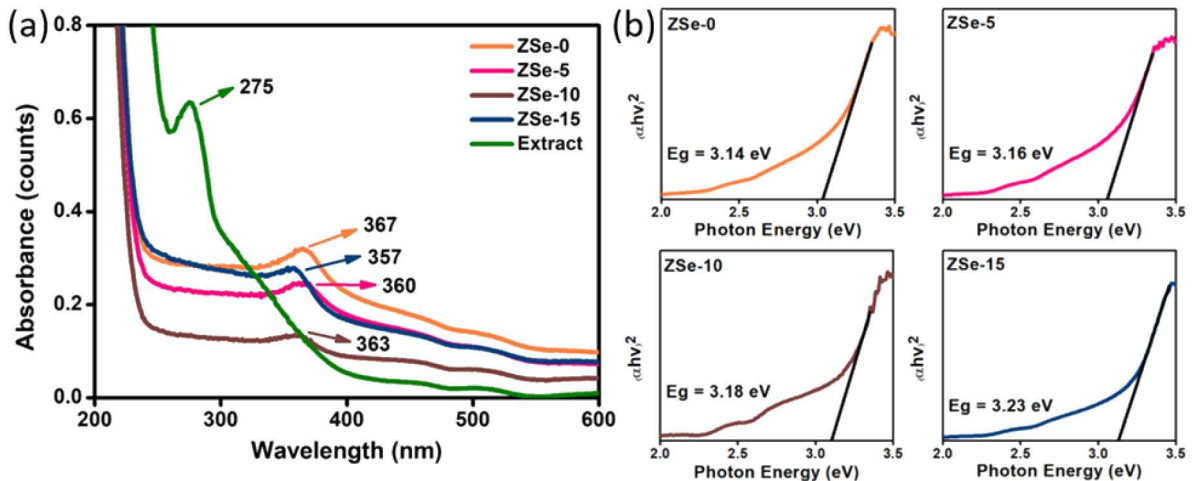


Figure 5. Absorbance spectra (a) and band gap energy curves (b) of Se-doped ZnO powders

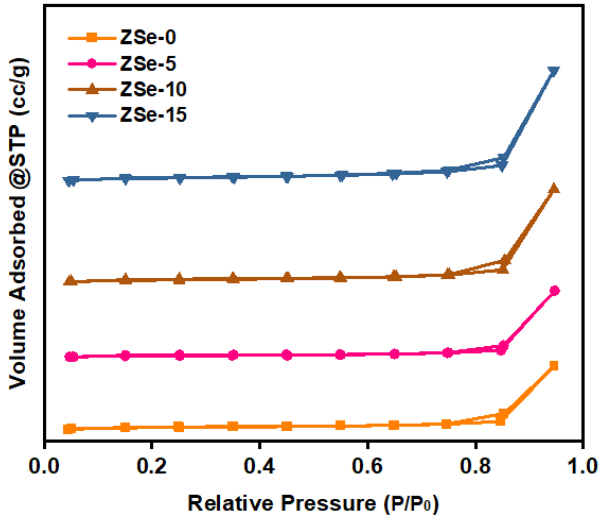


Figure 6. Adsorption-desorption isotherms of Se-doped ZnO samples

the amount of free charge content in the sample [14]. In addition, the observed decrease in particle size can also have influence on the band gap energy [27].

3.5. Adsorption-desorption analysis

Adsorption-desorption behaviour of the ZSe samples was evaluated with nitrogen gas at 77 K. The adsorption-desorption isotherms (Fig. 6) belong to a typical type IV, indicating the presence of mesopores. The adsorption-desorption curve for each ZSe shows a similar pattern, with a slight increase at low relative pressure (P/P_0) and then a spike increases when P/P_0 approaches one [33].

Surface area, pore size and total pore volume of the ZSe samples are given in Table 2. The samples with higher Se concentration (10 and 15 at.%) have higher

Table 2. Surface area (S_v), pore size and total pore volume (V_p) of Se-doped ZnO samples

Sample	S_v [m^2/g]	Pore size [nm]	V_p [cm^3/g]
ZSe-0	12.2	15.4	0.094
ZSe-5	10.1	19.5	0.098
ZSe-10	15.2	18.1	0.137
ZSe-15	18.4	17.9	0.164

surface area and larger total pore volume. This is consistent with the observed reduction in particle size in the doped ZnO powders. Kumar *et al.* [17] obtained similar results and reported that Se doping can increase the surface area and porosity of the Se^{2+}/ZnO samples synthesized by sol-gel method.

3.6. Degradation of 4-nitrophenol pollutant

Photocatalytic capability of the ZSe powders was evaluated by degrading the pollutant 4-nitrophenol (4-NP) under UV irradiation. The absorbance spectra of the degraded 4-NP solutions by the ZSe particles are shown in Fig. 7a. The characteristic absorption band of 4-NP exists at the wavelength of 400 nm [34]. There was a decrease in the absorbance of the 4-NP band with increasing irradiation time, indicating that the ZSe sample degradation process was successful. It occurs due to the direct UV-C rays hitting the ZSe particles with greater energy than the band gap energy [6]. Moreover, during the degradation process, the 4-NP solution changed from a yellow to a clear solution (Fig. 7b).

The reaction rate of the photocatalysis process can be determined by linear fitting of $\ln A/A_0$ versus irradiation time dependence, as presented in Fig. 8a. The ZSe samples with various Se contents have succeeded in degrading 4-NP pollutants which was confirmed by an increase in reaction rate constants from -0.0076 min^{-1}

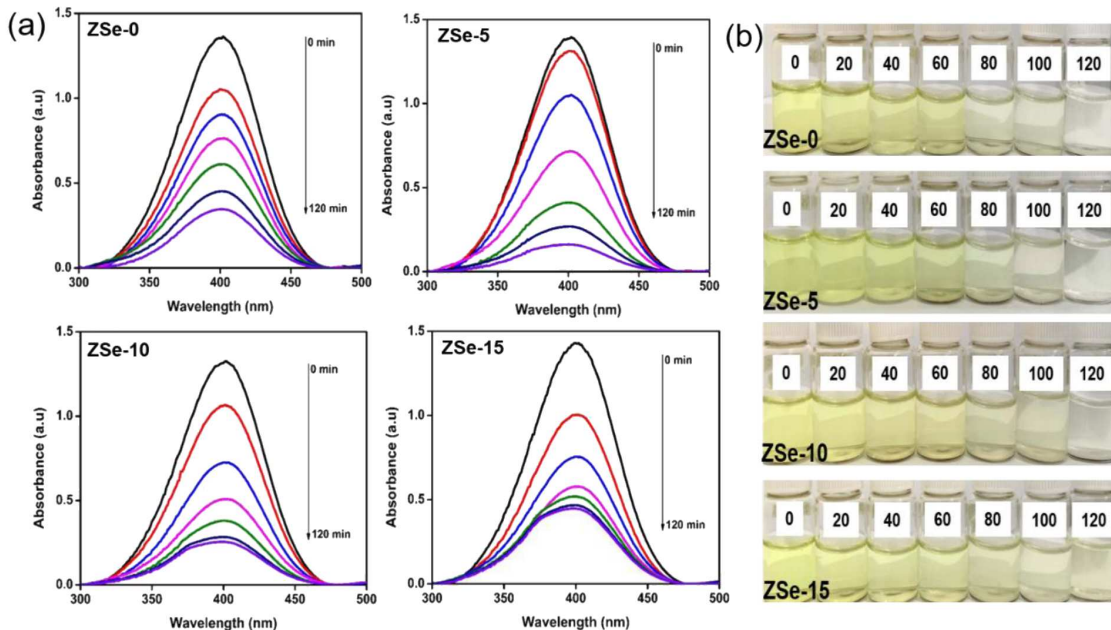


Figure 7. Absorbance curves (a) and changes in 4-NP pollutant solution (b) after degradation process by Se-doped ZnO

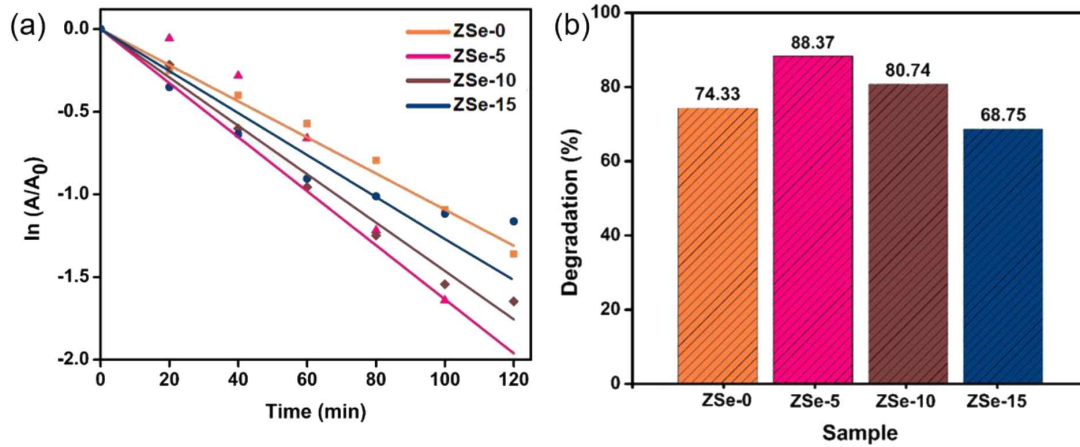


Figure 8. $\ln A/A_0$ vs. time plots (a) and photocatalytic efficiency (b) of Se-doped ZnO in degrading 4-NP pollutant

Table 3. Comparison of degradation efficiency of doped ZnO photocatalysts for various dye pollutants

Material	Dye	Light source (time)	Doping [at.%]	Degradation [%]	Ref.
Mg/ZnO 50 mg	Metilen Blue (3×10^{-5} M)	Sunlight (120 min)	0	55	[19]
			3	65	
			5	77	
			7	96	
Ag/ZnO 50 mg	RhB (5 ppm)	UV lamps (120 min)	0	41	[20]
			4	74	
Cu/ZnO 25 mg	MB (10 ppm)	Visible (100 min)	0	6	[35]
			1	54	
			2	69	
			3	73	
Se/ZnO 10 mg	4-NP (10 ppm)	UV lamps (120 min)	0	74	This work
			5	88	
			10	80	
			15	68	

(the sample ZSe-0) to -0.0218 min^{-1} (the sample ZSe-5). This is similar to the previous results of Lemecho *et al.* [35], who reported the degradation of methylene blue (MB) pollutants using ZnO and Cu-doped ZnO with reaction rates of 0.0063 and -0.0109 min^{-1} , respectively. It proves that doping effect can speed up reaction rates and increase the ability of ZnO photocatalysts to degrade pollutants.

The photocatalytic mechanism starts from the pair exciton that is produced when material is exposed to a light with energy greater than the bandgap energy. The formed pairs dissociate into electrons (e^-) in the conduction band and holes (h^+) in the valence band. Then, h^+ directly reacts with hydroxyl (OH^-) and H_2O to give hydroxyl radicals ($\bullet\text{OH}$). Meanwhile, e^- reduces oxygen (O_2) adsorbed on the ZnO surface into superoxide radicals ($\bullet\text{O}_2^-$). Therefore, the 4-NP pollutant can be photocatalytically decomposed by the resulting $\bullet\text{OH}$ and $\bullet\text{O}_2^-$ [23]. However, recombination of electrons and holes often occurs, which can prevent oxidation and reduction reactions from occurring on the surface of the photocatalytic material [5].

Figure 8b shows that the photocatalytic efficiency of the ZSe samples in degradation of 4-NP pollutant is higher than 65%. The ZSe-5 powder has the high-

est degradation rate of 88.4%. This is due to the optimum concentration of Se required for modification of the ZnO structure. So, selenium content of 5 at.% is considered as optimum. In addition, this result is supported by the largest pore size of 19.5 nm. Meanwhile, the ZSe-15 sample with the largest percentage of Se had the lowest photocatalytic efficiency of 68.8%. It is due to the increased structural defects in ZnO thereby reducing the photocatalytic performances [17]. Comparison of degradation efficiency of ZnO particles doped with different elements for various types of pollutants is given in Table 3. Based on these results, it can be concluded that the efficiency degradation of ZnO increases with the doping compared to the pure ZnO. The utilization of Se-doped ZnO combined with mediated matoa leaf extract as a mediator for the degradation of 4-NP pollutants has not been explored before. Therefore, this research can be developed for the application of photocatalysts in degrading pollutants that cause water pollution.

IV. Conclusions

Se-doped ZnO powders were prepared using a simple synthesis method mediated by matoa leaf extract. The

Se doping increases the lattice parameters in the crystal structure and widens the energy band gap. With increasing Se doping, the ZnO particle size decreases and the distribution becomes more uniform. It also increases the surface area and pore volume. The ZnO doped with 5 at.% Se produced the highest photocatalytic efficiency (88.4%) compared to the pure ZnO (74.3%). The high photocatalytic capability of the Se-doped ZnO can improve the quality of ZnO and reduce 4-NP pollution of wastewaters.

Acknowledgement: The research project is financially supported by the Ministry of Education, Culture, Research, and Technology of the Indonesian government through a research grant in 2023. The authors also express their gratitude to the Lembaga Penelitian dan Pengabdian Masyarakat (LPPM), Universitas Riau for supporting this work.

References

- J.L.D. De Tuesta, G.F. Pantuzza, A.M.T. Silva, P. Praça, J.L. Faria, H.T. Gomes, "Catalysts prepared with matured compost derived from mechanical-biological treatment plants for the wet peroxide oxidation of pollutants with different lipophilicity", *Catalysts*, **10** [11] (2020) 1243.
- D. Kalaimurugan, P. Sivasankar, K. Durairaj, M. Lakshmanamoorthy, S.A. Alharbi, S.A. Al Yousef, A. Chinathambi, S. Venkatesan, "Novel strategy for biodegradation of 4-nitrophenol by the immobilized cells of *Pseudomonas* sp. YPS3 with *Acacia* gum", *Saudi J. Biol. Sci.*, **28** [1] (2021) 833–839.
- S.D. Ashrafi, G.H. Safari, K. Sharafi, H. Kamani, J. Jaafari, "Adsorption of 4-Nitrophenol on calcium alginate-multiwall carbon nanotube beads: Modeling, kinetics, equilibriums and reusability studies", *Int. J. Biol. Macromol.*, **185** (2021) 66–76.
- X.X. Qiao, K. Yu, J.Y. Xu, Y.L. Cai, Y.F. Li, H.L. Cao, J. Lu, "Engineered nanoscale schwertmannites as Fenton-like catalysts for highly efficient degradation of nitrophenols", *Appl. Surf. Sci.*, **548** [15] (2021) 149248.
- J.J.R. Marquez, I. Levchuk, P.F. Ibañez, M. Sillanpää, "A critical review on application of photocatalysis for toxicity reduction of real wastewaters", *J. Clean Prod.*, **258** (2020) 120694.
- M.I. Din, R. Khalid, Z. Hussain, T. Hussain, A. Mujahid, J. Najeeb, F. Izhar, "Nanocatalytic assemblies for catalytic reduction of nitrophenols: A critical review," *Crit. Rev. Anal. Chem.*, **50** [4] (2020) 322–338.
- I. Medine-Ramírez, A. Hernández-Ramírez, M.L. Maya-Trevino, "Synthesis methods for photocatalytic materials", pp. 69–102 in *Photocatalytic Semiconductors*. Eds. A. Hernández-Ramírez, I. Medine-Ramírez, Springer, 2015.
- S.N.A.M. Sukri, K. Shameli, E.D. Mohamed Isa, N.A. Ismail, "Green synthesis of zinc oxide-based nanomaterials for photocatalytic studies: A mini review", *IOP Conf. Ser. Mater. Sci. Eng.*, **1051** [1] (2021) 012083.
- E. Mohammadi, M. Aliofkhaezai, M. Hasanpoor, M. Chipara, "Hierarchical and complex ZnO nanostructures by microwave-assisted synthesis: Morphologies, growth mechanism and classification", *Crit. Rev. Solid State Mater. Sci.*, **43** [6] (2018) 475–541.
- S. Mandar, D. Purnamsari, R. Zainul, "Catalytic activity of nano ZnO/Cu for degradation humic acid under illumination outdoor light", *J. Phys. Conf. Series*, **1481** [1] (2020) 012038.
- M. Carofiglio, S. Barui, V. Cauda, M. Laurenti, "Doped zinc oxide nanoparticles: Synthesis, characterization and potential use in nanomedicine", *Appl. Sci.*, **10** [15] (2020) 5194.
- S.Z. Umbaidillah, N.A.M. Asib, A.N. Afaah, M. Rusop, Z. Khusaimi, "A review on the effect of metal doped ZnO nanostructures on ultraviolet photoconductive sensor performance", *AIP Conf. Proc.*, **2151** [1] (2019) 020038.
- S.N.A. Sulaiman, M. Zaky Noh, N. Nadia Adnan, N. Bidin, S.N. Ab Razak, "Effects of photocatalytic activity of metal and non-metal doped TiO₂ for hydrogen production enhancement - A review", *J. Phys. Conf. Series*, **1027** [1] (2018) 012006.
- B.P. Nenavathu, A. Sharma, R. K. Dutta, "Se doped ZnO nanoparticles with improved catalytic activity in degradation of cholesterol", *J. Water Environ. Nanotech.*, **3** [4] (2018) 289–300.
- A. Ahmad, S. Ullah, W. Ahmad, Q. Yuan, R. Taj, A.U. Khan, A.U. Rahman, U.A. Khan, "Zinc oxide-selenium heterojunction composite: Synthesis, characterization and photo-induced antibacterial activity under visible light irradiation," *J. Photochem. Photobiol. B Biol.*, **203** (2020) 111743.
- A.S. Rini, Y. Rati, M. Agustin, Y. Hamzah, A.A. Umar, "Seed-mediated synthesis and photoelectric properties of selenium doped zinc oxide nanorods", *Sains Malaysiana*, **49** [12] (2020) 3055–3063.
- S. Kumar, S.K. Sharma, R.D. Kaushik, L.P. Purohit, "Chalcogen-doped zinc oxide nanoparticles for photocatalytic degradation of Rhodamine B under the irradiation of ultraviolet light", *Mater. Today Chem.*, **20** (2021) 100464.
- T. Algarni, N.A.Y. Abduh, A. Al Kahtani, A. Aouissi, "Photocatalytic degradation of some dyes under solar light irradiation using ZnO nanoparticles synthesized from *Rosmarinus officinalis* extract", *Green Chem. Let. Rev.*, **15** (2022) 460–473.
- R.E. Adam, H. Alnoor, G. Pozina, X. Liu, M. Willander, O. Nur, "Synthesis of Mg-doped ZnO NPs via a chemical low-temperature method and investigation of the efficient photocatalytic activity for the degradation of dyes under solar light", *Solid State Sci.*, **99** (2020) 106053.
- M. Saeed, M. Siddique, M. Ibrahim, N. Akram, M. Usman, M.A. Aleem, A. Baig, "Calotropis gigantea leaves assisted biosynthesis of ZnO and Ag@ ZnO catalysts for degradation of rhodamine B dye in aqueous medium", *Environ. Prog. Sustainable Energy*, **39** [4] (2020) e13408.
- R.A.R. Ahmad, Z. Harun, M.H.D. Othman, H. Basri, M.Z. Yunos, A. Ahmad, S.H.N. Akhair, A.Q.A. Rashid, F.H. Azhar, S.S. Alias, A.R. Ainuddin, "Biosynthesis of zinc oxide nanoparticles by using fruits extracts of *Ananas Comosus* and its antibacterial activity", *Malaysian J. Fundam. Appl. Sci.*, **15** [2] (2019) 268–273.
- M. Aminuzzaman, P.S. Ng, W.S. Goh, S. Ogawa, A. Watanabe, "Value-adding to dragon fruit (*Hylocereus polyrhizus*) peel biowaste: green synthesis of ZnO nanoparticles and their characterization", *Inorg. Nano-Metal Chem.*, **49** [11] (2019) 401–411.
- A.S. Rini, Y. Rati, R. Fadillah, R. Farma, L. Umar, Y. Soer-

- bakti, “Improved photocatalytic activity of ZnO film prepared via green synthesis method using red watermelon rind extract,” *Evergreen*, **9** [4] (2022) 1046–1055.
24. G.S. Prihanti, R.M.K. Katjasungkana, B.R. Novitasari, S.R. Amalia, A. Nurfajriana, S.M. Agustini, H. Cakrawati, D. Andari, “Antidiabetic potential of matoa bark extract (*Pometia pinnata*) in alloxan-induced diabetic male rat strain wistar (*Rattus norvegicus*)”, *Syst. Rev. Pharm.*, **11** [8] (2020) 88–97.
 25. A.A. Yahya, K.T. Rashid, M.Y. Ghadhban, N.E. Mousa, H.S. Majidi, I.K. Salih, Q.F. Alsalhy, “Removal of 4-nitrophenol from aqueous solution by using polyphenylsulfone-based blend membranes: Characterization and performance”, *Membranes*, **11** [3] (2021) 171.
 26. H. Sadiq, F. Sher, S. Sehar, E.C. Lima, S. Zhang, H.M.N. Iqbal, F. Zafar, M. Nuhanovic, “Green synthesis of ZnO nanoparticles from *Syzygium Cumini* leaves extract with robust photocatalysis applications”, *J. Mol. Liq.*, **335** (2021) 116567.
 27. K.K. Taha, M.M. Mustafa, H.A.M. Ahmed, S. Talab, “Selenium zinc oxide (Se/ZnO) nanoparticles: Synthesis, characterization, and photocatalytic activity”, *Zeitschrift für Naturforsch. - Sect. A J. Phys. Sci.*, **74** [12] (2019) 1043–1056.
 28. H. Neelamkodan, U. Megha, M.P. Binitha, “Enhanced green luminescence properties of Cu doped ZnO nano-flowers and their improved antibacterial activities”, *Process. Appl. Ceram.*, **17** [1] (2023) 81–90.
 29. M.C. Uribe-López, M.C. Hidalgo-López, R. López-González, D.M. Frías-Márquez, G. Núñez-Nogueira, D. Hernández-Castillo, M.A. Alvarez-Lemus, “Photocatalytic activity of ZnO nanoparticles and the role of the synthesis method on their physical and chemical properties”, *J. Photochem. Photobiol. A Chem.*, **404** (2021) 112866.
 30. Z. Xu, Q. Hou, F. Guo, Y. Li, C. Li, “Effects of strains on the electronic structure and optical properties of Ce-doped ZnO with interstitial H”, *Comput. Mater. Sci.*, **169** (2019) 109120.
 31. H.A. Salam, R. Sivaraj, K. Murugesan, V. Rajendran, “Photocatalytic potential of ZnO/TiO₂: A bionanocomposite from *Ocimum basilicum*”, *Bioinspir. Biomim. Nanobio-mater.*, **6** [1] (2018) 1–11.
 32. Y. Song, F. Yang, M. Ma, Y. Kang, A. Hui, Z. Quan, A. Wang, “Green synthesized Se-ZnO/attapulgitite nanocomposites using *Aloe vera* leaf extract: Characterization, antibacterial and antioxidant activities”, *LWT*, **165** (2022) 113762.
 33. F. Ambroz, T.J. Macdonald, V. Martis, I.P. Parkin, “Evaluation of the BET theory for the characterization of meso and microporous MOFs”, *Small Methods*, **2** [11] (2018) 1800173.
 34. V.P. Nguyen, H. Le Trung, T.H. Nguyen, D. Hoang, T.H. Tran, “Advancement of microwave-assisted biosynthesis for preparing Au nanoparticles using *ganoderma lucidum* extract and evaluation of their catalytic reduction of 4-nitrophenol”, *ACS Omega*, **6** [47] (2021) 32198–32207.
 35. B.A. Lemecho, F.K. Sabir, D.M. Andoshe, N.S. Gultom, D.H. Kuo, X. Chen, E. Mulugeta, T.D. Desissa, O.A. Zelekew, “Biogenic synthesis of Cu-doped ZnO photocatalyst for the removal of organic dye”, *Bioinorg. Chem. Appl.*, **2022** (2022) 8081494.